PERGAMON

International Journal of Heat and Mass Transfer 45 (2002) 2797–2814

International Journal of HEAT and MASS TRANSFER

www.elsevier.com/locate/ijhmt

Radiative transfer in real gases using reciprocal and forward Monte Carlo methods and a correlated-k approach

Lionel Tessé [a], Francis Dupoirieux [a,*], Bernard Zamuner [a], Jean Taine [b]

[a] *Fundamental and Applied Energetics Department (DEFA), Office National d'Études et de Recherches Aérospatiales, Chemin de la Hunière, 91761 Palaiseau Cedex, France*

[b] *Laboratoire d'Énergétique Moléculaire et Macroscopique, Combustion (EM2C), UPR 288 du CNRS et de l'ECP, École Centrale Paris, 92295 Châtenay-Malabry Cedex, France*

Received 20 November 2000; received in revised form 10 April 2001

Abstract

Two formulations of the Monte Carlo method based on the reciprocity principle, considered from both points of view of the reverse path and the exchanged power, are developed and discussed. Their results are compared to those of a conventional forward Monte Carlo approach in 1D benchmark cases involving gray media or actual gas-mixtures and different optical thicknesses and thermal conditions. Gas radiative properties are treated in a correlated manner by a CK model. Although these problems are 1D, the calculations have been carried out with 3D calculation grids in order to check the capacity of the different approaches for dealing with actual 3D systems. Advantages and drawbacks of the three formulations are discussed. In terms of computation time, it is not more expensive to obtain the results from the three approaches (with only one calculation) than to obtain the results from one given approach.

1. Introduction

Many methods have been developed to calculate radiative transfer for laboratory or engineering applications [1,2], such as the Monte Carlo method, the ray-tracing method, e.g., [3], the zone method, e.g., [4], the discrete ordinates or interpolation method, e.g., [5–11], the finite volume method, e.g., [12–15], the P_n method, e.g., [16,17], etc. However, as radiative transfer modeling requires accounting for some complex phenomena, such as spectral effects due to gases, wall bidirectional and bipolarized reflectivities, non-isotropic scattering, complex 3D geometries including islands, couplings with turbulent temperature and concentration fields, the Monte Carlo approach appears today to be the most suitable method because it allows all these phenomena to be taken into account without approximation and huge CPU time. The flexibility of this approach greatly offsets its reputation of slow convergence.

The Monte Carlo method has been widely used in radiative transfer since the first works in this domain [18–20], as mentioned in detailed reviews by Howell [21] and Farmer and Howell [22]. Many variance reduction procedures have been employed in particular cases [23–29]. Walters and Buckius [30,31] have developed a reverse approach, called the emission path method, based on the reciprocity principle, but using only its geometrical features to calculate the radiative flux at a given boundary point of a complex system. The optical path is then considered in a reverse manner. To our knowledge, Fournier [32], Cherkaoui et al. [33,34] and de Lataillade et al. [35] are the first authors to use the reciprocity principle from the point of view of the exchanged power. They have applied this Monte Carlo method in nearly isothermal conditions for 1D systems and have shown that, for these particular conditions, the computation time is much smaller than with a formulation of the conventional Monte Carlo approach. Hybrid methods have also been developed, i.e., with the zone method [36], with the diffusion approximation to treat optically thick media [22,37,38] or with the finite volume method [39].

* Corresponding author.

0017-9310/02/$ - see front matter
PII: S0017-9310(02)00009-1

Nomenclature

b	spectral band index
B, F, G	points of the system
c	index of crossing of a given cell by an optical path along this optical path
f, f_1, f_2, f_3	probability density functions
g, g_2	Gauss quadrature point indices
h	index of wall reflections along an optical path
i, j, q	cell indices
$I_\nu^0(T)$	equilibrium (or blackbody) spectral intensity (W m^{-2} (cm^{-1})$^{-1}$ sr^{-1})
k_{ibg}	pseudo-spectral absorption coefficient in the cell i (m^{-1})
l	length of the optical path or of one of its part (m)
L	distance between the walls in a slab (m)
m	cell index along an optical path
M	index of the current cell along an optical path
n	optical path index
N	total number of optical paths
N_i	number of optical paths originating from the cell i
N_{ij}	number of optical paths originating from the cell i and crossing or encountering the cell j
N_p	total number of crossings of a given cell by an optical path
N_{rc}	number of wall reflections along an optical path between the points B and F_c
N_S	number of elementary surfaces in the system
N_V	number of elementary volumes in the system
N_x, N_y, N_z	number of spatial discretizations in the directions x, y and z
$\mathscr{P}(\ )$	probability
P_i	radiative power in the cell i (W or W m^{-3})
P_{ij}^{ea}	power emitted by the cell i and absorbed by the cell j (W)
P_i^{e}	total power emitted by the cell i (W)
P_{ij}^{exch}	power exchanged between the cells i and j (W)
r	ratio of total equilibrium intensities
R, R_θ, R_φ	random numbers
s	position along a part of an optical path (m)
S	area (m^2)
t	computation time (s)
T_i, T_{c_s}, T_{w}	temperature of the cell i, of the slab center, of the walls of the slab (K)
V_i	volume of the cell i (m^3)
x, y, z	Cartesian coordinates (m)

Greek symbols

α_j, $\alpha_{j\nu}$	total, spectral absorptivity in the cell j
Δ	initial direction of the optical path
$\Delta\nu_b$	width of the spectral band b (cm^{-1})
$\varepsilon_{\mathrm{w}j\nu}$	spectral emissivity of the wall j
θ	polar angle
$\kappa_{i\nu}$	spectral absorption coefficient of the cell i (m^{-1})
ν	wavenumber (cm^{-1})
$\sigma(\ )$	standard deviation
τ_l	cutoff level
$\tau_\nu(BF)$	spectral transmissivity between the points B and F
φ	circumferential angle
ω_g	weight associated with the gth Gauss quadrature point
Ω	solid angle (sr)

Subscripts

w	refers to a wall

Superscript

$\widetilde{(\ )}$	statistical estimation (mean over the contributions of some or all the optical paths)

The most accurate models of gas radiative properties are the line-by-line approach, considered as a reference, and, in practice, narrow band models of which advantages and limitations have been widely discussed by Taine and Soufiani [40]. Liu and Tiwari [41] have explicitly used a statistical narrow-band model and have pointed out the importance of the spectral correlations effects, easily introduced in a Monte Carlo approach. Fournier [32], Cherkaoui et al. [33,34] and de Lataillade et al. [35] have deduced the probability distribution functions of the absorption coefficient from the parameters of this model.

The aim of the present paper is to compare three formulations of the Monte Carlo method. One is a formulation of the conventional forward Monte Carlo approach often cited in the literature; the two others are based on the reciprocity principle, from the points of view of the power exchanged between two cells and of the forward and reverse ways to describe an optical path. In all cases involving actual gas-mixtures, gas

radiative properties are treated in a correlated manner by a CK model [42–45] based on the parameters of Soufiani and Taine [46].

The three considered formulations of the Monte Carlo method are detailed in Section 2, in which their physical bases are also discussed. The implementation techniques of these three approaches are given in Section 3. In Section 4, the results obtained from the different formulations are compared in several benchmark cases, for which reference solutions exist. The behaviors of these three Monte Carlo formulations in many different conditions are then analyzed and a methodology for the best use of them is deduced.

2. Reciprocal and forward Monte Carlo formulations

In this paper, three different formulations of the Monte Carlo method are presented and compared. Two of them, called here the reciprocal methods, are based on the exchange formulation of radiative transfer which fulfills systematically the reciprocity principle. The other one is a conventional Forward Method (FM). In this approach, an optical path, which is stochastically generated from a point B to a point G, is used only for the transport of radiative energy from the point B to the point G, i.e., in the forward direction. In the reciprocal approaches, the same optical path is used to calculate directly the power exchanged between the points B and G, i.e., the transport of radiative energy in both forward and reverse directions. In Section 2.1, the exchange formulation of radiative transfer which gives rise to the reciprocal approaches is presented in terms of Probability Density Functions (PDF) which allow a statistical resolution, detailed in Section 2.2. The behaviors of the three approaches are discussed in Section 2.3.

2.1. Exchange formulation of radiative transfer

Let us consider an enclosure with non-isothermal opaque walls, containing a non-isothermal, heterogeneous, absorbing and emitting medium. The medium and the walls are divided into N_V elementary volumes and N_S elementary surfaces, respectively, both of which are called cells in the following. Each cell is assumed to be isothermal, homogeneous and characterized by uniform radiative properties.

The main idea of the exchange formulation of radiative transfer is that the radiative power (or radiative flux) in the cell i can be written as a sum of exchange terms with all the other cells j, i.e.,

$$P_i = \sum_{j=1}^{N_V+N_S} P_{ij}^{\text{exch}} = \sum_{j=1}^{N_V+N_S} -P_{ji}^{\text{exch}}, \tag{1}$$

where P_{ij}^{exch} is the radiative power exchanged between the cells i and j, i.e., the difference between the power emitted by the cell j and absorbed by the cell i and the power emitted by the cell i and absorbed by the cell j. If both cells i and j are volumes (see Fig. 1), P_{ij}^{exch} is given by

$$P_{ij}^{\text{exch}} = \int_0^{+\infty} \kappa_{iv}\left[I_v^0(T_j) - I_v^0(T_i)\right] \int_{V_i} \int_{4\pi} \sum_{c=1}^{N_p} \tau_v(BF_c) \times \left[\int_0^{l_{jc}} \kappa_{jv} \exp\left(-\kappa_{jv} s_{jc}\right) \mathrm{d}s_{jc}\right] \mathrm{d}\Omega_i \, \mathrm{d}V_i \, \mathrm{d}v, \tag{2}$$

where $I_v^0(T)$ is the equilibrium spectral intensity and κ_{iv} the spectral absorption coefficient relative to the cell i. N_p represents the total number of crossings of the cell j by a given optical path issued from the cell i. $\tau_v(BF_c)$ is the spectral transmissivity between the source point B associated with $\mathrm{d}V_i$ and F_c the cth inlet point in the cell j of a given optical path. s_{jc} is the abscissa, taken from F_c, of the current point G_c in the cell j for the cth crossing. l_{jc} represents the length of the cth crossing of the cell j by a given optical path. $\mathrm{d}\Omega_i$ is an elementary solid angle issued from the source point B and centered around a direction Δ. The spectral transmissivity is given by

$$\tau_v(BF_c) = \exp\left(-\sum_{m=1}^{M_c-1} \kappa_{mv} l_m\right) \prod_{h=1}^{N_{rc}} (1 - \varepsilon_{whv}), \tag{3}$$

where l_m is the distance traveled through the cell m; $m = 1$ and $m = M_c$ correspond, respectively, to the first cell crossed by an optical path (the cell i) and the last one for the cth crossing (the cell j). N_{rc} is the number of wall reflections along an optical path between the points B and F_c, h the index of wall reflections along this optical path and ε_{whv} the local wall spectral emissivity.

In Eq. (2) the integration over the volume V_j has been replaced by integrations over the solid angle 4π and the length l_{jc}, i.e.,

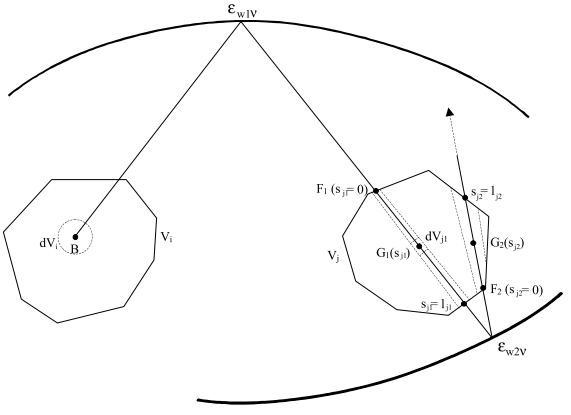

Fig. 1. Coupled elementary cells.

$$\frac{\mathrm{d}V_{jc}}{l_{BG_c}^2} = \mathrm{d}s_{jc}\,\mathrm{d}\Omega_i, \tag{4}$$

where l_{BG_c} is the length of an optical path between the source point B and the current point G_c. After analytical integration over the length l_{jc}, the radiative power exchanged between the cells i and j becomes

$$P_{ij}^{\mathrm{exch}} = \int_0^{+\infty} \kappa_{iv} I_v^0(T_i) \left(\frac{I_v^0(T_j)}{I_v^0(T_i)} - 1 \right) \times \int_{V_i} \int_{4\pi} \sum_{c=1}^{N_p} \tau_v(BF_c)\alpha_{jcv}\,\mathrm{d}\Omega_i\,\mathrm{d}V_i\,\mathrm{d}v, \tag{5}$$

where α_{jcv} is the spectral absorptivity associated with the column of length l_{jc} and defined by

$$\alpha_{jcv} = 1 - \exp(-\kappa_{jv} l_{jc}). \tag{6}$$

In this formulation, an elementary exchange is an exchange between an elementary volume $\mathrm{d}V_i$ of the cell i and an elementary column of length l_{jc} crossing the cell j. The reciprocity principle is clearly fulfilled by Eq. (5): the ratio of the spectral power emitted by a cell i and absorbed by a cell j to the spectral power emitted by j and absorbed by i is equal to the ratio of the equilibrium spectral intensities $I_v^0(T_i)/I_v^0(T_j)$.

Since the point B, the direction Δ and the wavenumber v are statistically independent, the corresponding joint PDF $f_i(B,\Delta,v)$ is equal to the product of the PDF, f_{1i}, f_{2i} and f_{3i}, associated with B, Δ and v, i.e.,

$$f_i(B,\Delta,v)\,\mathrm{d}V_i\,\mathrm{d}\Omega_i\,\mathrm{d}v = f_{1i}(B)\,\mathrm{d}V_i\,f_{2i}(\Delta)\,\mathrm{d}\Omega_i\,f_{3i}(v)\,\mathrm{d}v, \tag{7a}$$

$$= \frac{1}{V_i}\,\mathrm{d}V_i\,\frac{1}{4\pi}\,\mathrm{d}\Omega_i\,\frac{\kappa_{iv} I_v^0(T_i)}{\int_0^{+\infty} \kappa_{iv} I_v^0(T_i)\,\mathrm{d}v}\,\mathrm{d}v, \tag{7b}$$

$$= \frac{\kappa_{iv} I_v^0(T_i)\,\mathrm{d}\Omega_i\,\mathrm{d}V_i\,\mathrm{d}v}{P_i^{\mathrm{e}}}, \tag{7c}$$

where P_i^{e} is the total power emitted by the whole volume V_i, over the whole spectrum for all directions, without taking into account self-absorption by this volume. By combining Eqs. (5) and (7c), we obtain

$$P_{ij}^{\mathrm{exch}} = P_i^{\mathrm{e}} \int_0^{+\infty} \left(\frac{I_v^0(T_j)}{I_v^0(T_i)} - 1 \right) \times \int_{V_i} \int_{4\pi} \sum_{c=1}^{N_p} \tau_v(BF_c)\alpha_{jcv} f_i(B,\Delta,v)\,\mathrm{d}\Omega_i\,\mathrm{d}V_i\,\mathrm{d}v. \tag{8}$$

Eqs. (6)–(8) have been established for a volume–volume exchange, but similar relations can be easily deduced for volume–surface, surface–volume or surface–surface exchanges. If the cell j is a surface, the medium spectral absorptivity α_{jcv} is changed to the wall spectral emissivity $\varepsilon_{\mathrm{w}jv}$. If the cell i is a surface, integrations over the volume V_i and the solid angle 4π are replaced by integrations over the surface S_i and the solid angle 2π in Eq. (8) and the PDF becomes

$$f_i(B,\Delta,v)\,\mathrm{d}S_i\,\mathrm{d}\Omega_i\,\mathrm{d}v = f_{1i}(B)\,\mathrm{d}S_i\,f_{2i}(\Delta)\,\mathrm{d}\Omega_i\,f_{3i}(v)\,\mathrm{d}v, \tag{9a}$$

$$= \frac{1}{S_i}\,\mathrm{d}S_i\,\frac{\cos(\theta_i)}{\pi}\,\mathrm{d}\Omega_i\,\frac{\varepsilon_{\mathrm{w}iv} I_v^0(T_i)}{\int_0^{+\infty} \varepsilon_{\mathrm{w}iv} I_v^0(T_i)\,\mathrm{d}v}\,\mathrm{d}v, \tag{9b}$$

$$= \frac{\varepsilon_{\mathrm{w}iv} I_v^0(T_i)\cos(\theta_i)\,\mathrm{d}\Omega_i\,\mathrm{d}S_i\,\mathrm{d}v}{P_i^{\mathrm{e}}}, \tag{9c}$$

where P_i^{e} is now the total power emitted by the surface S_i.

2.2. Monte Carlo method approximation

A Monte Carlo method is a statistical method based on the simulation of a large number of stochastic events. Each stochastic event represents a possible realization of the considered physical phenomenon. The solution of the problem is obtained by averaging the contributions of all the stochastic events. In radiative transfer, a stochastic event is an optical path. In the FM, some power associated with an optical path is emitted by a cell and partially absorbed by each cell crossed by the optical path. In the reciprocal Monte Carlo approaches, the power exchanged between a source cell (cell from which an optical path is built) and each cell crossed by the optical path is directly calculated, as explained previously, along each optical path.

According to Eq. (8), each optical path is characterized by a source point associated with the source cell $\mathrm{d}V_i$ or $\mathrm{d}S_i$, a direction Δ and a wavenumber v. That means that the stochastic generation of an optical path requires the independent stochastic generations of a source point, a direction and a wavenumber according to the three PDF defined in Eqs. (7a) and (7b) or (9a) and (9b). Details about these generations are given in Section 3.

If a large number N_i of optical paths are stochastically generated from the cell i using the PDF given by Eqs. (7a) and (7b) or (9a) and (9b), a large number of them, called N_{ij}, cross or encounter the cell j and each of these N_{ij} optical paths provides one value for:

(i) P_{ij}^{ea}, the power emitted by the cell i and absorbed by the cell j in the FM;
(ii) P_{ij}^{exch}, the power exchanged between the cells i and j in the reciprocal approaches.

Statistical estimations of P_{ij}^{ea} and P_{ij}^{exch}, noted $\widetilde{P}_{ij}^{\mathrm{ea}}$ and $\widetilde{P}_{ij}^{\mathrm{exch}}$ in the following, are obtained by averaging the contributions of all the N_i optical paths (but only N_{ij} optical paths give rise to a non-zero contribution). Obviously, the standard deviations of these quantities decrease as the number N_i of optical paths increases. $\widetilde{P}_{ij}^{\mathrm{ea}}$ is simply given by

$$\widetilde{P}_{ij}^{\mathrm{ea}} = \frac{P_i^{\mathrm{e}}}{N_i} \sum_{n=1}^{N_{ij}} \sum_{c=1}^{N_p} \tau_{v_n}(B_{in} F_{jcn}) \alpha_{jcv_n}. \quad (10)$$

According to Eq. (8), $\widetilde{P}_{ij}^{\mathrm{exch}}$ is expressed as

$$\widetilde{P}_{ij}^{\mathrm{exch}} = \frac{P_i^{\mathrm{e}}}{N_i} \sum_{n=1}^{N_{ij}} \left[\frac{I_{v_n}^0(T_j)}{I_{v_n}^0(T_i)} - 1 \right] \sum_{c=1}^{N_p} \tau_{v_n}(B_{in} F_{jcn}) \alpha_{jcv_n}. \quad (11)$$

In Eqs. (10) and (11), the absorption is treated as a continuous phenomenon in a deterministic manner (Beer law). In this hybrid Monte Carlo approach the factor $\tau_{v_n}(B_{in} F_{jcn}) \alpha_{jcv_n}$ is deduced from Eqs. (3) and (6). In a pure Monte Carlo approach, the absorption would be stochastically treated. That means that the absorption would be total in only one cell j which would be randomly chosen using an appropriate PDF not defined here. Therefore, the product $\tau_{v_n}(B_{in} F_{jcn}) \alpha_{jcv_n}$ would be equal to 1 in this only cell j and equal to 0 in all the other cells crossed by an optical path. The analytical treatment used here in this hybrid approach gives rise to lower standard deviations in the results, since it decreases the number of stochastic variables [22].

In Eq. (11), the term including the ratio of the equilibrium spectral intensities corresponds to the reverse direction of an optical path, with which emission from the cell j and absorption by the cell i are associated. The other term corresponds to the forward direction of an optical path, with which emission from the cell i and absorption by the cell j are associated.

At this stage, the FM and two reciprocal Monte Carlo formulations based on Eq. (2) can be implemented in order to calculate the radiative power (or the radiative flux) in the cell q. In the FM, only the power transported in the forward direction of an optical path is taken into account (see Fig. 2). The radiative power in the cell q, which is crossed or encountered by optical paths originating from all the system cells i, including the cell q, is obtained by making the balance between absorption and emission in this cell after all the optical paths have been generated from all the cells i. A statistical estimation of the radiative power in the cell q is then expressed as

$$\widetilde{P}_q^{\mathrm{FM}} = \sum_{i=1}^{N_V+N_S} \widetilde{P}_{iq}^{\mathrm{ea}} - P_q^{\mathrm{e}}. \quad (12)$$

In the first reciprocal approach, called the Emission Reciprocity Method (ERM), the radiative power is calculated in the cell q, which is the source of the optical paths (see Fig. 3). In other terms, only the powers exchanged between the cell q and all the cells, crossed or encountered by the optical paths originating from the cell q, are considered. A statistical estimation of the radiative power in the cell q is then given by

$$\widetilde{P}_q^{\mathrm{ERM}} = \sum_{j=1}^{N_V+N_S} \widetilde{P}_{qj}^{\mathrm{exch}}. \quad (13)$$

Substituting Eq. (11) into Eq. (13) yields

$$\widetilde{P}_q^{\mathrm{ERM}} = \frac{P_q^{\mathrm{e}}}{N_q} \sum_{n=1}^{N_q} \sum_{m=1}^{M_n} \left[\frac{I_{v_n}^0(T_m)}{I_{v_n}^0(T_q)} - 1 \right] \tau_{v_n}(B_{qn} F_{mn}) \alpha_{mv_n}, \quad (14)$$

where $m = 1$ designates the cell q and $m = M_n$ the last cell crossed by the nth optical path originating from the cell q. Eq. (14) shows that the statistical estimation of the radiative power (or radiative flux) in the cell q can be calculated as soon as all the optical paths originating from the cell q have been generated. Thus, the ERM allows accurate calculation of the radiative power (or radiative flux) in only one cell by simply allocating a

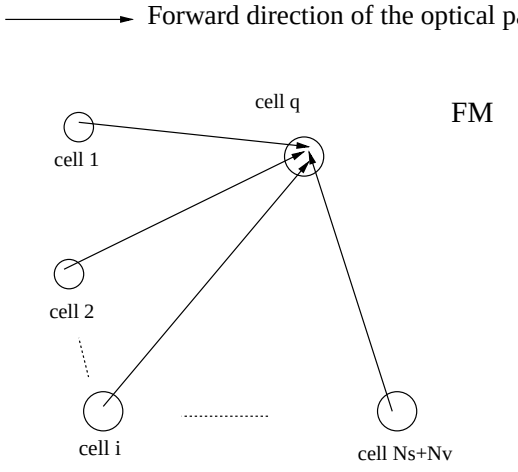

Fig. 2. Principle of the calculation of the radiative power in the cell q in the FM (the emitted power is calculated analytically).

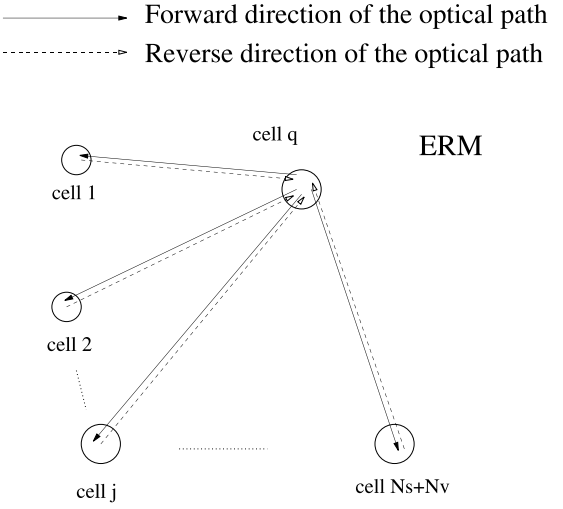

Fig. 3. Principle of the calculation of the radiative power in the cell q in the ERM.

large number of optical paths starting from this cell. This property has been used in the reverse method developed by Walters and Buckius [30,31]. However, these authors do not use the reciprocity principle in terms of exchanged power; they only describe the optical path in a reverse manner. It is worth noting that, in the ERM, the expression of the power emitted by the cell q is exactly P_q^e; indeed, as the energy is conserved along an optical path the sum $\sum_{m=1}^{M_n} \tau_{v_n}(B_{qn}F_{mn})\alpha_{mv_n}$ in the negative term of Eq. (14) is equal to 1. Therefore, the error in the ERM is only due to the statistical calculation of the absorption term, like in the FM.

In the second reciprocal formulation, called the Absorption Reciprocity Method (ARM), the radiative power is calculated in the cell q which is crossed or encountered by optical paths issued from all the system cells i including the cell q (see Fig. 4). In other words, the optical paths along which the exchanged powers are considered cross or encounter the cell where the radiative power is calculated. Therefore, a statistical estimation of the radiative power in the cell q is given by

$$\widetilde{P}_q^{\mathrm{ARM}} = \sum_{i=1}^{N_V+N_S} -\widetilde{P}_{iq}^{\mathrm{exch}}. \tag{15}$$

It is worth noting that $\widetilde{P}_{ij}^{\mathrm{exch}}$ used in the ERM becomes strictly equal to $-\widetilde{P}_{ji}^{\mathrm{exch}}$ used in the ARM only when the total number N of optical paths tends to infinity. Moreover, in the ARM like in the FM, the statistical estimation of the radiative power (or radiative flux) in the cell q can only be calculated when all the optical paths originating from all the system cells i including the cell q have been generated. The expression obtained by substituting Eq. (11) into Eq. (15) can be derived from Eq. (12) corresponding to the FM, if we consider the following relation, arising from the reciprocity principle

$$P_q^e = \sum_{i=1}^{N_V+N_S} \lim_{N_i\to+\infty} \frac{P_i^e}{N_i} \sum_{n=1}^{N_{iq}} \frac{I_{v_n}^0(T_q)}{I_{v_n}^0(T_i)} \sum_{c=1}^{N_p} \tau_{v_n}(B_{in}F_{qcn})\alpha_{qcv_n}. \tag{16}$$

In the ARM, the power emitted by the cell q is statistically reconstructed, by using the reciprocity principle, from the power carried in the forward direction and absorbed by the cell q. The paradoxical advantage of this formulation lies in the following: although the emitted power is approximated, the exchanged power is correctly evaluated since the reciprocity principle is used and therefore the ratio of the emitted and absorbed powers is exact.

In conclusion, the main interest of a reciprocal approach (ERM or ARM) is that the power exchanged between two cells at the same temperature is rigorously null, as shown in Eqs. (11) and (13)–(15). This property is only statistically verified by the FM. On the other hand, it will be established in Section 2.3 that the energy conservation principle, rigorously fulfilled by the FM, is only statistically verified by the reciprocal approaches developed here. However, it will be also established that the approaches developed here based on the reciprocity principle lead in many cases to more accurate results than those of the FM.

2.3. Behaviors of the three Monte Carlo formulations

A simple fictitious case displays how the errors in the three formulations depend on physical conditions. Let us consider an isolated system consisting of two homogeneous gray zones exchanging radiative energy, the zone 1 being included inside the zone 2 of which the size is large. We assume that the external boundary of the zone 2 is perfectly reflecting.

The total power emitted by the zone i ($i = 1, 2$) is noted P_i^e. A reciprocity factor r is defined as the ratio of the total equilibrium intensities I_2^0/I_1^0. We also introduce α_i which is the fraction of the power emitted by the zone i and absorbed by the zone i itself. As soon as the parameters α_i are known, the problem is solved. In fact, $\widetilde{\alpha}_i$ results directly from the stochastic generations of the source point and of the direction. Our purpose is to understand how the error on the radiative power is influenced by the statistics, in other words, to determine how this error depends on the statistical error on $\widetilde{\alpha}_i$.

The radiative powers in the zones 1 and 2 are defined in the three previous methods (FM, ERM and ARM) by the expressions

$$\widetilde{P}_1^{\mathrm{FM}} = P_2^e(1-\widetilde{\alpha}_2) - P_1^e(1-\widetilde{\alpha}_1), \quad \widetilde{P}_2^{\mathrm{FM}} = -\widetilde{P}_1^{\mathrm{FM}}, \tag{17}$$

$$\widetilde{P}_1^{\mathrm{ERM}} = P_1^e(1-\widetilde{\alpha}_1)(r-1), \quad \widetilde{P}_2^{\mathrm{ERM}} = -\widetilde{P}_1^{\mathrm{ARM}}, \tag{18}$$

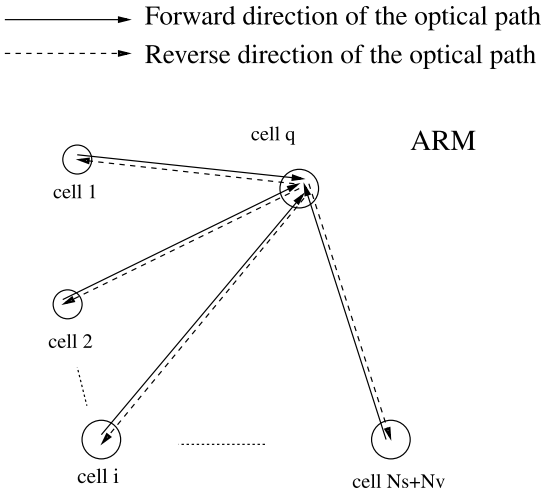

Fig. 4. Principle of the calculation of the radiative power in the cell q in the ARM.

$$\widetilde{P}_1^{\mathrm{ARM}} = P_2^{\mathrm{e}}(1-\widetilde{\alpha}_2)\left(1-\frac{1}{r}\right), \quad \widetilde{P}_2^{\mathrm{ARM}} = -\widetilde{P}_1^{\mathrm{ERM}}. \tag{19}$$

According to these equations, the energy of the system is rigorously conserved in the FM ($\widetilde{P}_1^{\mathrm{FM}} + \widetilde{P}_2^{\mathrm{FM}} = 0$). But, in the ERM and the ARM, the sum $\widetilde{P}_1 + \widetilde{P}_2$ depends on the stochastic values of $\widetilde{\alpha}_1$ and $\widetilde{\alpha}_2$. In these two reciprocal approaches, the energy is statistically conserved. In the same manner, the reciprocity principle is only statistically fulfilled in the FM, i.e., $P_2^{\mathrm{e}}(1-\widetilde{\alpha}_2)$ becomes strictly equal to $rP_1^{\mathrm{e}}(1-\widetilde{\alpha}_1)$ only when the total number N of stochastic optical paths tends to infinity (obviously, when the total number of optical paths tends to infinity, the three methods become equivalent). The reciprocity principle is obviously fulfilled by ARM and ERM, which are derived from Eq. (5). It can be verified in Eqs. (18) and (19) that the ratio of the power emitted by the zone 2 and absorbed by the zone 1 to the power emitted by the zone 1 and absorbed by the zone 2 is rigorously equal to r.

The standard deviations, noted σ, are straightforwardly deduced from the previous equations

$$\begin{aligned}
&\sigma\left(\widetilde{P}_1^{\mathrm{FM}}\right) = \sqrt{\left[P_2^{\mathrm{e}}\sigma(\widetilde{\alpha}_2)\right]^2 + \left[P_1^{\mathrm{e}}\sigma(\widetilde{\alpha}_1)\right]^2},\\
&\sigma\left(\widetilde{P}_2^{\mathrm{FM}}\right) = \sigma\left(\widetilde{P}_1^{\mathrm{FM}}\right),
\end{aligned} \tag{20}$$

$$\begin{aligned}
&\sigma\left(\widetilde{P}_1^{\mathrm{ERM}}\right) = P_1^{\mathrm{e}}|r-1|\sigma(\widetilde{\alpha}_1),\\
&\sigma\left(\widetilde{P}_2^{\mathrm{ERM}}\right) = \sigma\left(\widetilde{P}_1^{\mathrm{ARM}}\right),
\end{aligned} \tag{21}$$

$$\begin{aligned}
&\sigma\left(\widetilde{P}_1^{\mathrm{ARM}}\right) = P_2^{\mathrm{e}}\left|1-\frac{1}{r}\right|\sigma(\widetilde{\alpha}_2),\\
&\sigma\left(\widetilde{P}_2^{\mathrm{ARM}}\right) = \sigma\left(\widetilde{P}_1^{\mathrm{ERM}}\right).
\end{aligned} \tag{22}$$

If r is close to 1 (nearly isothermal configurations) the ARM and the ERM give the smallest error. Since the radiative power is close to zero, application of the reciprocity principle ensures that the numerical values of $\widetilde{P}_1$ and $\widetilde{P}_2$ will be close to zero no matter what the values of $\widetilde{\alpha}_1$ and $\widetilde{\alpha}_2$ are. That corroborates the results obtained by Fournier [32] and Cherkaoui et al. [33,34], who also use a reciprocal approach.

If r is far from 1, for instance $r \ll 1$ when zone 1 is a flame surrounded by zone 2 filled with air at room temperature, the error of the FM can become lower than the error of the ARM and the ERM in one of the two zones. Of course, the best result is obtained by combining the ARM with the ERM, i.e., by considering the result given by the ARM in one zone and the result given by the ERM in the other one. However, the analysis is much more complex when dealing with a large number of zones. For instance, the ARM can be recommended if we consider the exchange of a given cell with a given zone, but the ERM can be better for the exchange with another zone. If we consider all the exchanges, the FM may also be the most accurate formulation. The standard deviations of the three methods have to be compared in each cell.

It is worth noting at this point that many other formulations combining FM, ARM, ERM do exist. Some of them, though entirely based on the reciprocity principle, fulfill rigorously the energy conservation principle [32–34]. These methods deal with a huge $(N_V + N_S) \times (N_V + N_S)$ matrix of which the coefficients are the local exchanged powers $\widetilde{P}_{ij}^{\mathrm{exch}}$. Therefore they cannot be applied to 3D systems containing typically 10^4 cells.

3. Implementation of the methods

The Monte Carlo method is based on the simulation of a large number N of optical paths. In the three formulations developed in this paper, the cell from which an optical path is built is not generated stochastically. The number of optical paths originating from each cell are calculated in a deterministic manner. Two spatial distribution techniques have been developed. One is characterized by a Non-Uniform spatial Distribution (NUD) of the optical path source points in the calculation domain; the number N_i of optical paths originating from the cell i is proportional to P_i^{e}. The other technique uses a Uniform spatial Distribution (UD) of the optical path source points, which leads to the same number of optical paths originating from all the cells. The three Monte Carlo formulations, described in Section 2, can be associated with either the NUD or the UD technique.

To build each optical path, the wavenumber, the source point and the direction, characterizing each optical path, have to be generated stochastically. The wavenumber ν_n is deduced from R, a uniform random number in [0-1], following the implicit expression

$$R = \int_0^{\nu_n} f_{3i}(\nu)\,\mathrm{d}\nu = \frac{\int_0^{\nu_n} \kappa_{i\nu} I_\nu^0(T_i)\,\mathrm{d}\nu}{\int_0^{+\infty} \kappa_{i\nu} I_\nu^0(T_i)\,\mathrm{d}\nu}. \tag{23}$$

Details are given in the Appendix A about the implementation of the CK model for absorbing-emitting gases. To stochastically generate a source point B in a cell of any shape, some points are randomly picked in the smallest parallelepiped containing the cell, assuming that all the points of the parallelepiped have the same probability to be picked, until one is located inside the cell. This point is then taken as the source point. Two angles θ and φ are randomly generated to define the initial direction of the optical path. These angles are expressed as functions of two independent uniform [0-1] random numbers R_θ and R_φ. For a volume element, these functions are

$$\theta = \arccos(1-2R_\theta), \tag{24a}$$

$$\varphi = 2\pi R_\varphi, \tag{24b}$$

and, for an opaque surface element with diffuse emissivity, they become

$$\theta = \arccos\left(\sqrt{R_\theta}\right), \tag{25a}$$

$$\varphi = 2\pi R_\varphi. \tag{25b}$$

The optical path is then completely defined. All the stochastic generations detailed here are common to the three methods.

In the same way, the same optical paths are used in the three approaches, but differently. In the three methods, an optical path is always built step by step in the forward direction until the power carried in this direction becomes less than a cutoff level, expressed as a transmissivity τ_l (the choice of this cutoff level is discussed in Section 4). Indeed, in order to decrease the number of stochastic variables and thus the global standard deviation of the numerical solution [22], the absorption is treated as a continuous phenomenon in a deterministic manner. Therefore, each volumic cell j crossed N_p times by an optical path absorbs a part of the power, transported in the forward direction, equal to

$$P_{ijn}^{\mathrm{ea}} = \frac{P_i^{\mathrm{e}}}{N_i} \sum_{c=1}^{N_p} \tau_{v_n}(B_{in} F_{jcn}) \alpha_{jcv_n}. \tag{26}$$

In the FM, this amount of power is the contribution of this optical path to the power absorbed by the cell j. When the optical path encounters a wall, a fraction, equal to the wall spectral emissivity, of the power carried in the forward direction is absorbed by the wall, i.e., the medium spectral absorptivity α_{jcv_n} is changed to the wall spectral emissivity $\varepsilon_{\mathrm{w}jv_n}$ in Eq. (26). The remaining power leaves the wall in a direction which is randomly generated according to Eqs. (25a) and (25b). When the power carried in the forward direction reaches the value of the cutoff level, the remaining power is then totally absorbed by the cell following, in the forward direction, the one where the cutoff level has been reached.

In each cell j where power transported in the forward direction is absorbed, the power exchanged between the source cell i and this absorbing cell is easily calculated. In the ERM, the contribution of this optical path to the radiative power in the cell i is equal to

$$P_{ijn}^{\mathrm{exch}} = P_{ijn}^{\mathrm{ea}} \left[\frac{I_{v_n}^0(T_j)}{I_{v_n}^0(T_i)} - 1 \right]. \tag{27}$$

In the same way, in the ARM, the contribution of this optical path to the radiative power in the cell j is equal to $-P_{ijn}^{\mathrm{exch}}$. When all the optical paths have been built from all the cells, the final step consists in summing, in each cell, all the contributions taken into account in the different methods.

It is worth noting that the results given by the three methods are obtained simultaneously with only one calculation. Another important point to note is that it is not more expensive, in terms of computation time, to obtain the results from the three methods than from only one. Indeed, the initialization steps (calculation of the total emitted power in each cell, stochastic generations of source points, initial directions and wavenumbers) and the geometrical construction of the optical paths, which are common to the three methods, take most of the calculation time. In other words, these methods differ only by the final step for which the CPU time is negligible.

4. Results and discussion

A non-isothermal, emitting and absorbing medium between two parallel infinite isothermal semi-reflecting opaque walls, perpendicular to the x direction and characterized by diffuse emissivities, defines a benchmark case since the radiative power profile and the fluxes on the walls are given by well-known expressions (see [47, Eq. (VII.110)] or [48]), called here reference solution. Although this system is 1D, all the calculations here have been carried out with 3D calculation grids in order to check the capacity of the methods for dealing with actual 3D systems. The chosen computation system is a cube of edge length L. To simulate the infinite transverse dimensions of the 1D benchmark case along the y and z directions, total specular reflection conditions (i.e., symmetry conditions) are considered for the four lateral faces of the cube. If N_y and N_z are the numbers of meshes in the y and z directions, the radiative powers and the wall fluxes are calculated in N_yN_z cells at a given x location. All these calculations lead, at a given x location, not only to a mean result for each quantity, but also to the corresponding standard deviation σ.

In all the calculations, the temperature profile $T(x)$ always has a symmetric parabolic shape, but different values of the temperature T_{c_s} of the medium center and of the wall temperature T_{w} have been considered.

Several random number generators have been tested, and insensitivity of the results to the generator used has been observed. All the calculations presented in this paper have been performed with a combined multiple recursive generator developed by L'Ecuyer [49] and called MRG32k3a.

4.1. Case of a gray medium

Although no actual medium is gray, the gray assumption is useful since it allows the optical thickness of a medium to be controlled.

First, the influence of the total number N of optical paths has been studied. For a given case, the product of the result variance σ^2 and the computation time t is independent of N, as shown for instance in Fig. 5. In practice, the computation time t is proportional to the total number of cells crossed by all the optical paths, i.e., t is proportional to N, to the mean length of the optical paths and to the number of spatial discretizations per unit distance averaged over the three directions. Then, for all the considered conditions (optical thickness, temperature profile and wall emissivity) the influences of the total number N of optical paths, the value of the cutoff level τ_l and the numbers of spatial discretizations N_x, N_y and N_z have been studied in order to choose suitable values for these parameters.

The three Monte Carlo formulations studied in Section 2 are applied to the first five cases defined in Table 1. The wall emissivity ε_w is equal to 0.8 and the cube edge length L to 0.2 m. The total number N of optical paths has been adjusted in each case in order to use the same computation time, about 600 s on a single NEC SX5 processor. The comparison of standard deviations σ obtained from the different approaches is then significant since the performance of a Monte Carlo method is defined as the product of the computation time t and the variance σ^2 [22]. It is worth noting that the computation time would be shorter if a simpler and faster locating procedure, allowed by the actual 1D geometry, were used. Indeed, calculations have been carried out with a complex locating procedure developed in order to deal with 3D grid made up of irregular meshes closed by 12 faces.

Results relative to case 1, which corresponds to a semi-transparent medium of optical thickness equal to 2, and obtained from the ERM, ARM and FM formulations, associated with the UD and NUD of the optical

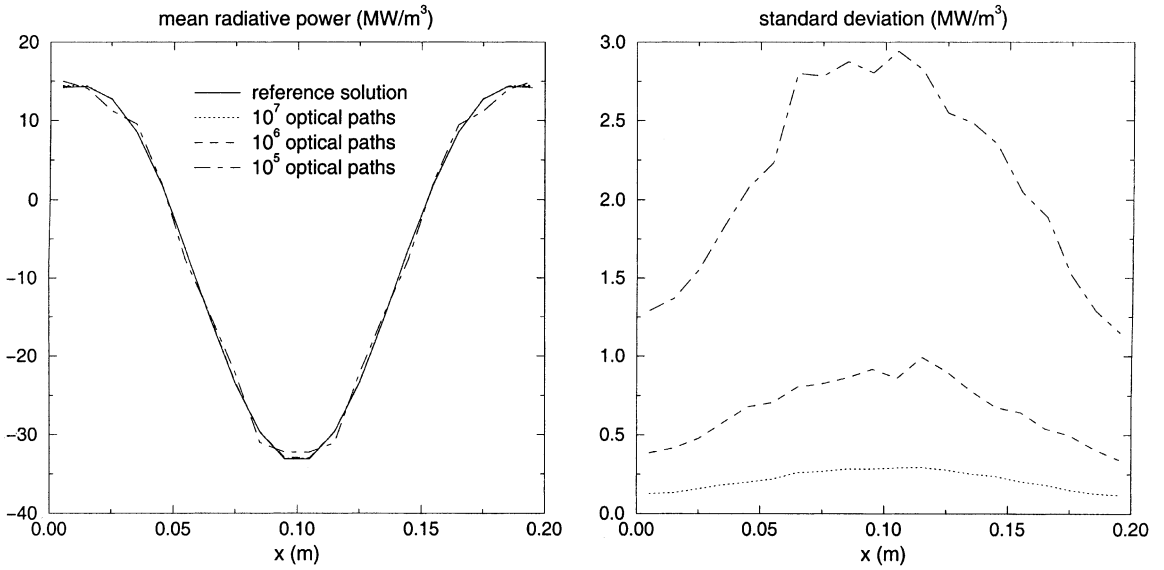

Fig. 5. Influence of the total number N of optical paths on mean power and on standard deviation over N_yN_z values of $\widetilde{P}$ (case 1, FM–NUD).

Table 1
Benchmark cases

	Case 1	Case 2	Case 3	Case 4	Case 5	Case 6	Case 7
κL	2	0.1	40	2	2	Actual gases	Actual gases
L (m)	0.2	0.2	0.2	0.2	0.2	0.2	4
ε_w	0.8	0.8	0.8	0.8	0.8	1	1
T_{c_s} (K)	2500	2500	2500	500	300	2500	2500
T_w (K)	500	500	500	2500	290	500	500
$N_x \times N_y \times N_z$	$20 \times 20 \times 20$	$20 \times 20 \times 20$	$400 \times 5 \times 4$	$20 \times 20 \times 20$	$20 \times 20 \times 20$	$20 \times 20 \times 20$	$20 \times 20 \times 20$
$N \times 10^{-6}$	1	0.2	1.35	1	1	1	1.8
$\tau_l \times 100$	1	0.1	0.1	1	1	1	0.1
t (s)	≈600	≈600	≈600	≈600	≈600	≈600	≈600

path source points, are shown in Figs. 6 and 7 and Table 2. Calculated mean radiative powers agree with the reference solution. Differences appear only in the obtained standard deviation values. FM results depend slightly on the spatial distribution of the optical path source points. Nevertheless, with this formulation, the NUD based on the powers emitted by the cells leads to the smallest standard deviations, which was expected in particular in the hot region. On the contrary, both ARM and ERM results are very sensitive to the spatial distribution of the optical path source points. In particular, as the number of optical paths originating from a cold region is small, large standard deviation values are observed for ERM in Fig. 6 in this type of region. Reciprocally, rather good results are obtained from this approach in the hot region. The same explanation can be

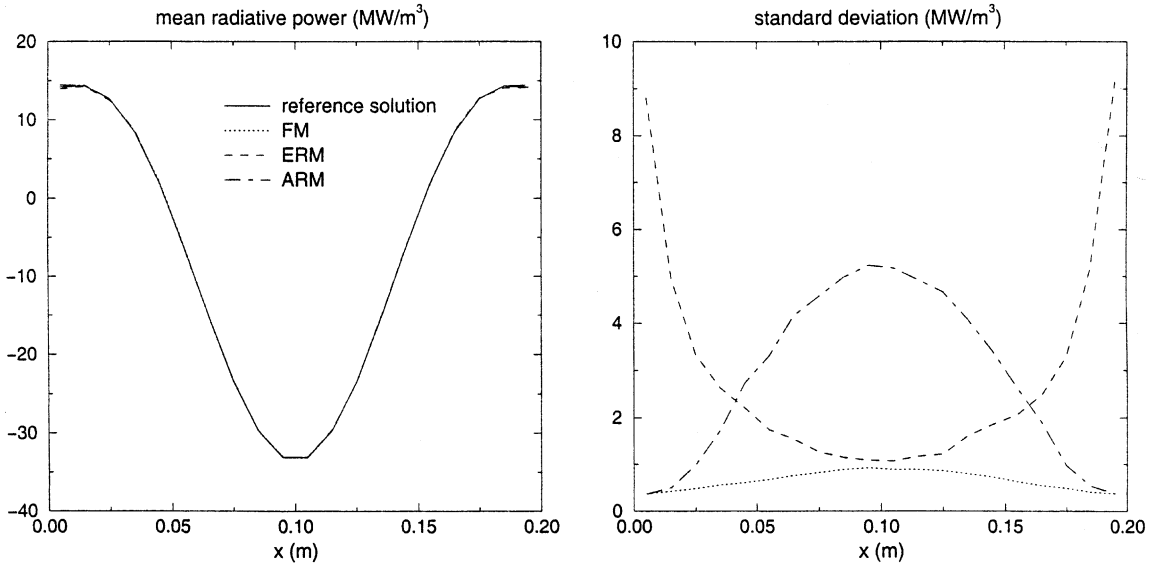

Fig. 6. Mean power value and standard deviation over N_yN_z values of $\widetilde{P}$ (case 1, NUD).

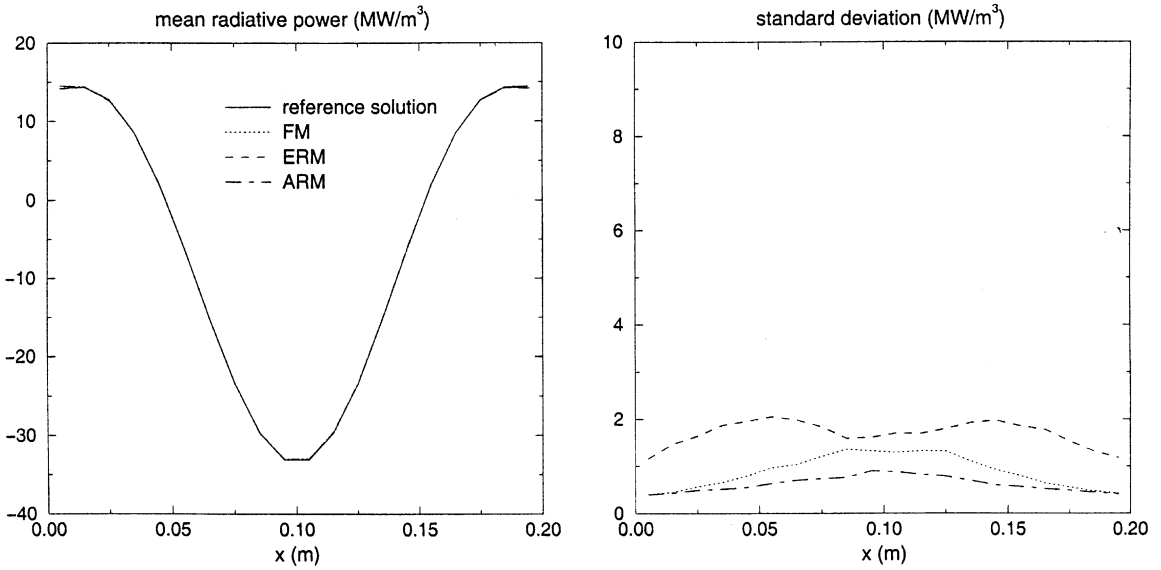

Fig. 7. Mean power value and standard deviation over N_yN_z values of $\widetilde{P}$ (case 1, UD).

Table 2
Flux averaged over the two walls and, in parentheses, corresponding standard deviation

	Case 1	Case 2	Case 3	Case 4	Case 5	Case 6	Case 7
Reference solution	560.5 kW m^{-2}	159.9 kW m^{-2}	7.057 kW m^{-2}	−1306 kW m^{-2}	24.26 W m^{-2}	54.04 kW m^{-2}	195.9 kW m^{-2}
FM							
NUD	553.0 (22.8)	159.5 (8.8)	6.399 (1.760)	−1312 (23)	20.15 (14.28)	54.03 (2.67)	195.7 (15.0)
UD	553.8 (25.2)	159.7 (11.7)	6.884 (0.204)	−1312 (34)	20.54 (14.01)	53.98 (3.02)	194.7 (17.7)
ERM							
NUD	562.6 (87.9)	161.0 (38.3)	6.805 (2.722)	−1306 (4)	24.21 (0.25)	53.41 (83.43)	134.1 (420.9)
UD	558.5 (12.4)	160.2 (15.1)	6.989 (0.267)	−1306 (10)	24.21 (0.33)	52.46 (39.93)	182.5 (283.7)
ARM							
NUD	553.1 (22.7)	159.6 (8.6)	6.601 (1.078)	−1292 (292)	23.97 (1.01)	54.03 (2.62)	195.7 (14.8)
UD	553.8 (25.2)	159.7 (11.7)	6.888 (0.159)	−1293 (52)	24.00 (0.96)	53.98 (2.98)	194.8 (17.6)

given in the hot region for the ARM formulation associated with the NUD of the optical path source points. Most of the optical paths which cross the hot zone originate from the cold and warm regions and their numbers are too small to accurately treat the hot region. To summarize, it is better, in general, to use the UD with the ARM and ERM formulations and the NUD with the FM formulation.

Case 2 corresponds to an optically thin medium between very absorbing walls. The required cutoff level is then smaller than the one previously used (10^{-3} instead of 10^{-2}). Indeed, if the cutoff criterion is too large, for many optical paths the cumulative transmissivity along the path reaches the cutoff level value just after encountering a wall, and the remaining power is then placed in cells close to the walls. The accumulation of the remaining power in a cell leads to a large error in the calculation of the absorption in this cell. With a wall emissivity equal to 0 or 1, this problem disappears. As a consequence, to obtain the same computation time in case 2 than in case 1, the total number N of optical paths must then be lower in case 2 than in case 1, as shown in Table 1, since the mean length of the optical paths is enhanced, due to both the lower medium optical thickness and the lower cutoff level value. As in case 1, the power is emitted by the medium, mainly by its hot central zone. But unlike case 1, in which absorption is mainly due to the whole medium, the power is mainly absorbed by the cold walls in case 2. Therefore, the reciprocal approaches are not suitable in case 2 characterized by an exchange between two strongly non-isothermal zones. The best results are then obtained from the FM–NUD formulation in the whole medium and on the walls, as illustrated by Fig. 8 and Table 2. The ARM formulation leads to the worst results in the medium center where absorption is negligible. ARM–UD is practically as accurate as FM–NUD in the vicinity of the walls, where the ratio absorption/emission is much larger than in the hot region. The ERM approach is always unsatisfactory in case 2.

For case 3, in which the medium is optically thick, a calculation grid with a refined spatial discretization in direction x is required in order to have a better description of the temperature profile since a cell is assumed to be isothermal. Moreover, a low value of the cutoff level must be used in order to increase the mean length of the optical paths. A cutoff level equal to 0.01 leads to an overestimation of the absorption in the hot zone and to an underestimation in the cold zones, because the optical paths mainly originating from the hot zone do not reach the cold ones. Furthermore, a small increase of the total number N of optical paths is required since the mean length of the optical paths is shorter than in the previous cases, although the cutoff criterion is smaller. In these optical and thermal conditions, all the calculated mean radiative power fields do

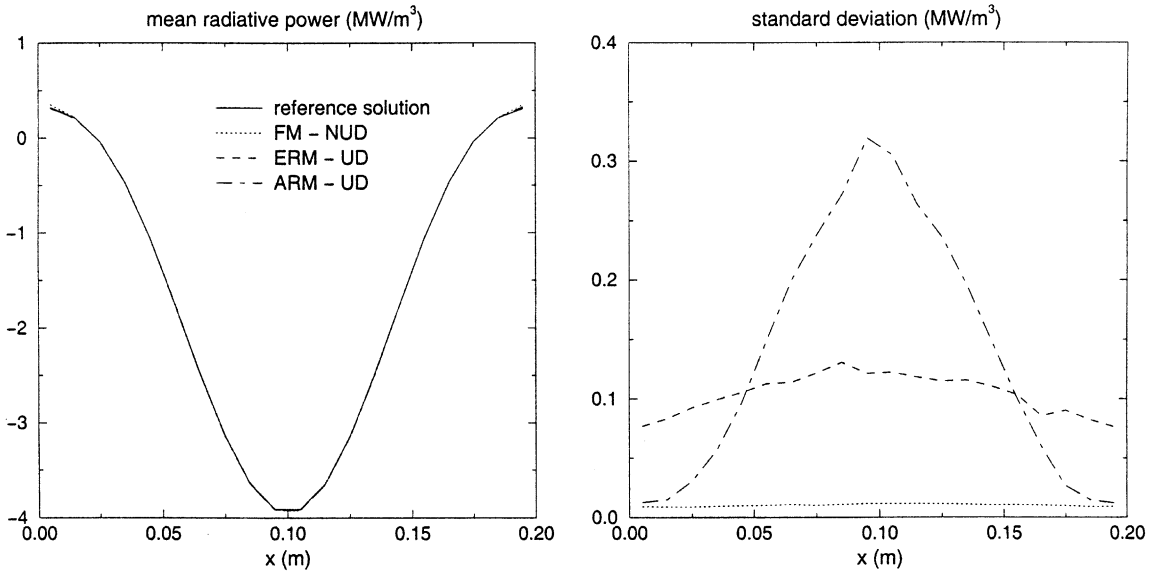

Fig. 8. Mean power value and standard deviation over N_yN_z values of $\widetilde{P}$ (case 2).

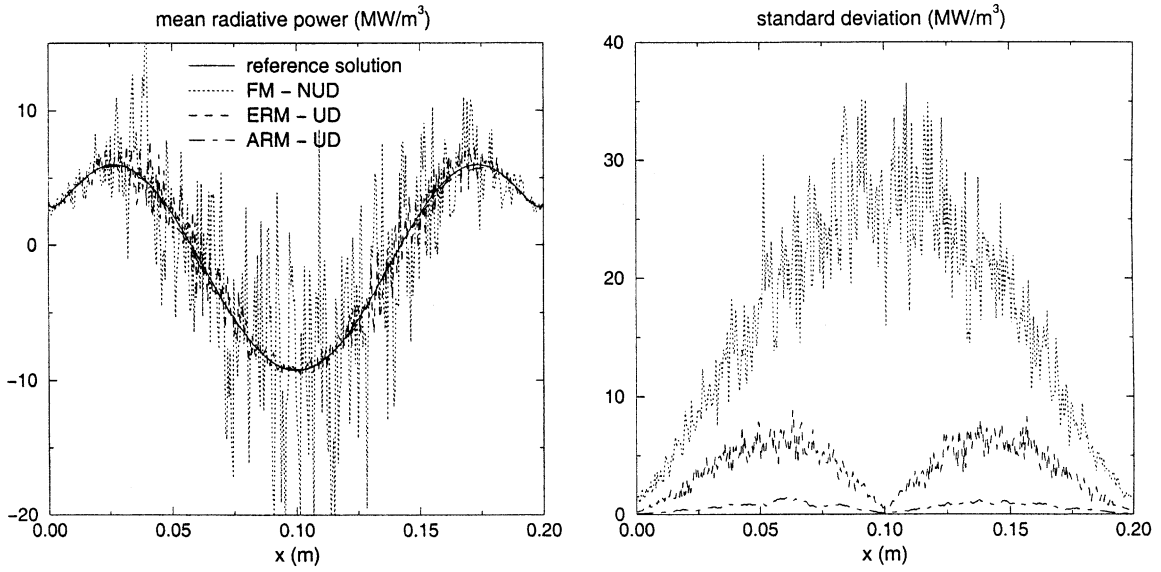

Fig. 9. Mean power value and standard deviation over N_yN_z values of $\widetilde{P}$ (case 3).

not agree with the reference solution, as shown in Fig. 9. The fluctuations of the three results are due to the required large number of spatial discretizations between the walls. The medium is so optically thick that exchanges are restricted to neighboring cells, which are nearly isothermal. That is the reason why the two reciprocal formulations are better than FM. As the whole medium and the walls are very absorbing, ARM is better than ERM everywhere. However, in the center of the medium, where emission is an important phenomenon, ERM provides good results as well. In the center of the medium, ARM standard deviation is 200 times smaller than the FM one, i.e., to obtain the same standard deviation, the FM requires a computation time 40 000 times larger than the ARM one.

Case 4 is defined by hot walls separated by a cold absorbing medium. The FM formulation produces the best results, as illustrated by Fig. 10, for the same reason

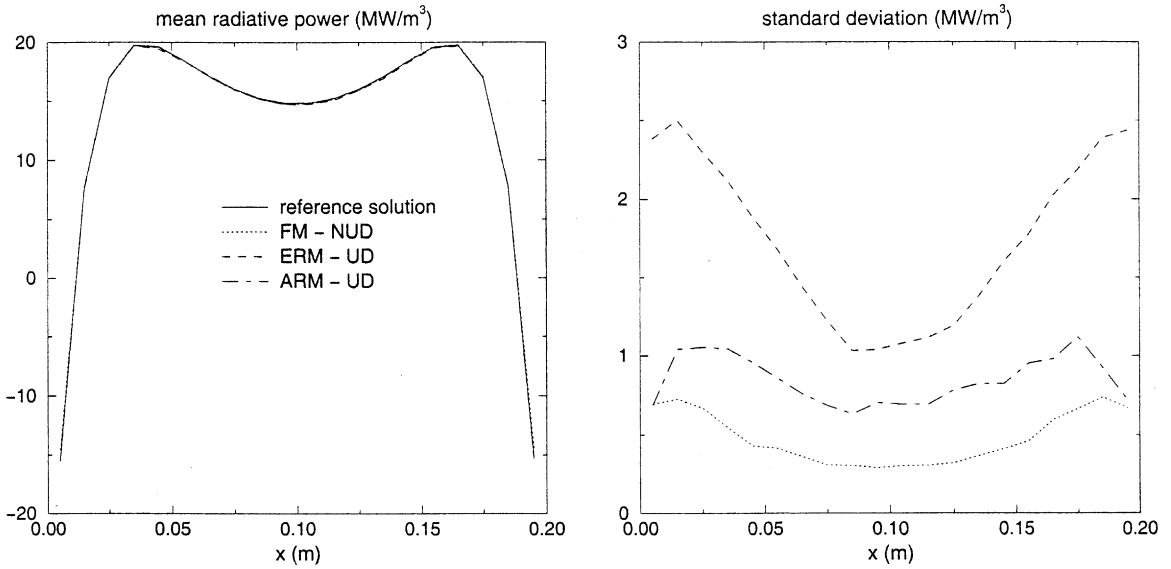

Fig. 10. Mean power value and standard deviation over N_yN_z values of $\widetilde{P}$ (case 4).

than in case 2, i.e., case 4 is characterized by exchanges between strongly non-isothermal zones. ARM results are better than ERM ones because the medium is more absorbing than emitting.

Case 5 is a thermal configuration similar to that of Fournier [32] and Cherkaoui et al. [33,34]. As the system is nearly isothermal, the reciprocal methods are more efficient, as shown in Fig. 11. These results confirm those of the previous authors. The standard deviation relative to ARM results is roughly 25 times smaller than the one relative to FM results.

The formulation associated with the spatial distribution of the optical path source points, which leads to the best results for the power field and the wall fluxes, is given in Table 3 for each case. The most suitable formulations for wall flux calculations can differ from those associated with power calculations. In case 1, corresponding to a semi-transparent medium characterized

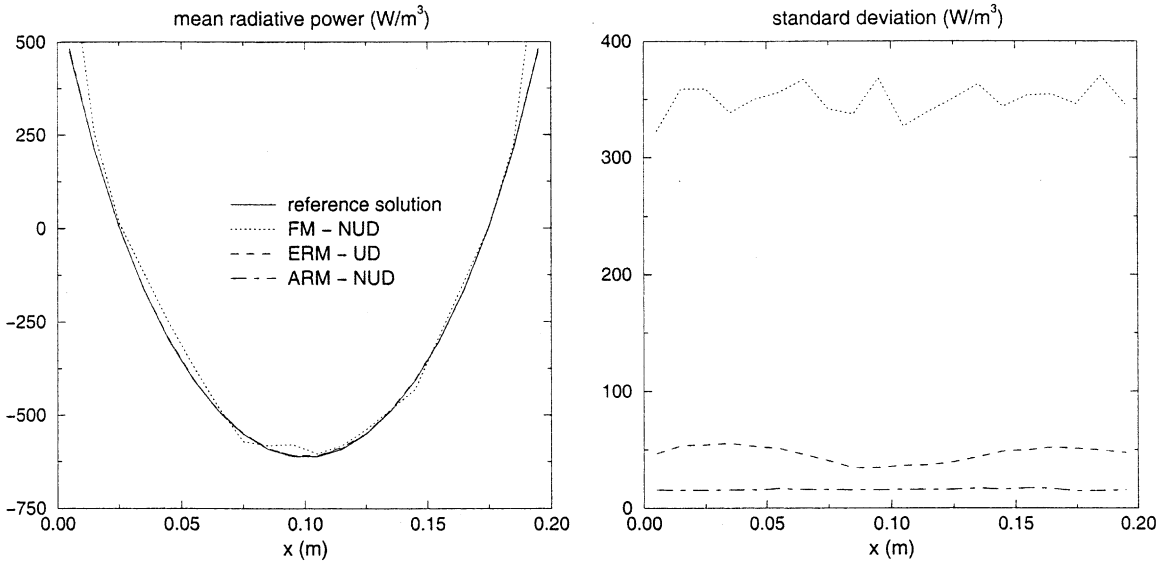

Fig. 11. Mean power value and standard deviation over N_yN_z values of $\widetilde{P}$ (case 5).

Table 3
Best approaches for radiative power and wall flux calculations

	Case 1	Case 2	Case 3	Case 4	Case 5	Case 6	Case 7
Power	ARM–UD or FM–NUD	FM–NUD	ARM–UD	FM–NUD	ARM–NUD or UD	FM–NUD	ARM–UD near the walls and ERM–UD elsewhere
Flux	ERM–UD	ARM or FM–NUD	ARM–UD	ERM–NUD	ERM–NUD or UD	ARM or FM–NUD	ARM or FM–NUD or UD

by an intermediate value of the optical thickness, the layer between the system center and a wall has an equivalent optical thickness of 1.8 (Hottel's equivalent radius). Consequently a significant part of radiation emitted by the hot central region reaches the walls. In this case, the ERM–UD formulation is the most suitable for the wall flux calculation: on one hand, absorption of radiation emitted by the hot region is taken into account correctly by the reciprocity principle; on the other hand, the number of optical paths originating from a wall is much larger with the UD than with the NUD. In case 2, corresponding to a thin medium, as for power calculation, the ARM formulation is equivalent to the FM one in the vicinity of the walls. The emission by the hot region is then accurately determined, especially with the NUD of the optical path source points. In case 3, relative to a very thick medium, the same analysis as for power calculations leads to the conclusion that the ARM–UD is the best formulation for the wall flux calculation. In case 4, since the walls are practically the only radiation source, the ERM–NUD formulation is the most suitable approach for the wall flux calculation.

4.2. Case of a real gas

Two benchmark cases, similar to those of [50] and also defined in Table 1, allow comparison of the behaviors of the three Monte Carlo formulations with actual gas mixtures. Gas radiative properties are treated in a correlated manner by a CK model [42–45] based on the parameters of Soufiani and Taine [46]. The reference solution is also integrated over the whole spectrum according to the CK model. The influence of the optical thickness is replaced by that of the cube edge length L. The wall emissivity ε_w is equal to 1. The CO_2–H_2O–N_2 mixture, at atmospheric pressure, is characterized by CO_2 and H_2O molar fractions equal to 0.116 and 0.155, respectively. The total number N of optical paths is adjusted in order to have the same computation time for all the calculations.

Case 6 corresponds to a thin medium, as the case 2. Indeed, according to the Hottel's charts [4], the total emissivities of the whole medium assumed to be isothermal at 2500 and 500 K are equal to 0.03 and 0.15, respectively. Consequently, the behaviors of the three Monte Carlo formulations are similar to those observed in the case 2, as shown in Figs. 12 and 8. As in case 2, the ARM is inaccurate in the medium core. In this region, the ERM is rather accurate but its standard deviation becomes larger in the regions close to the walls. The FM is the most accurate of the three methods.

In case 7, the total emissivity of the whole medium ranges from 0.19 at 2500 K to 0.50 at 700 K. For these intermediate values of the equivalent optical thickness, an interesting conclusion can be drawn: the best ap-

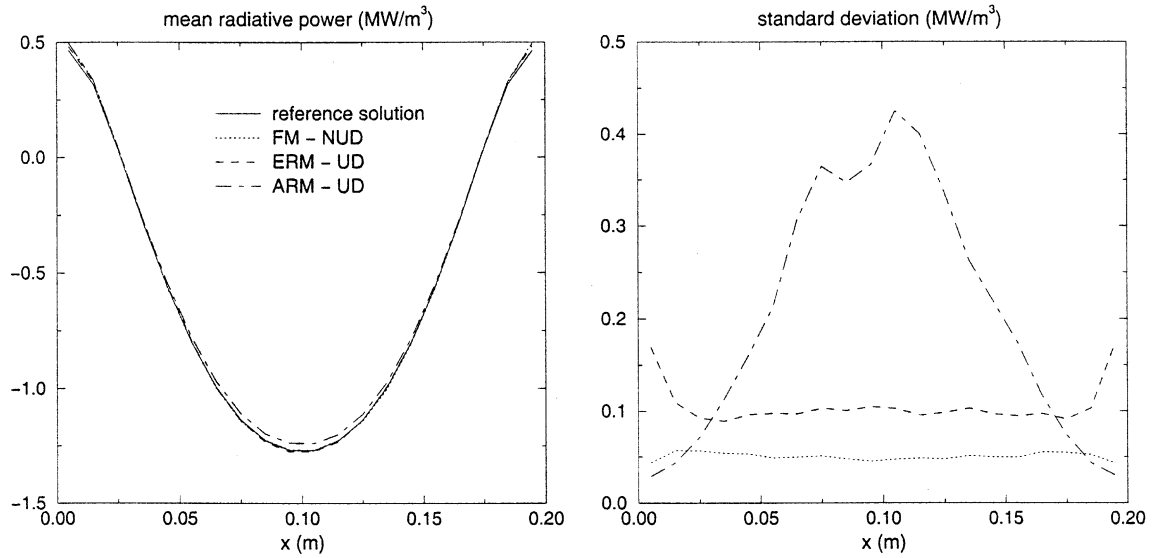

Fig. 12. Mean power value and standard deviation over $N_y N_z$ values of $\widetilde{P}$ (case 6).

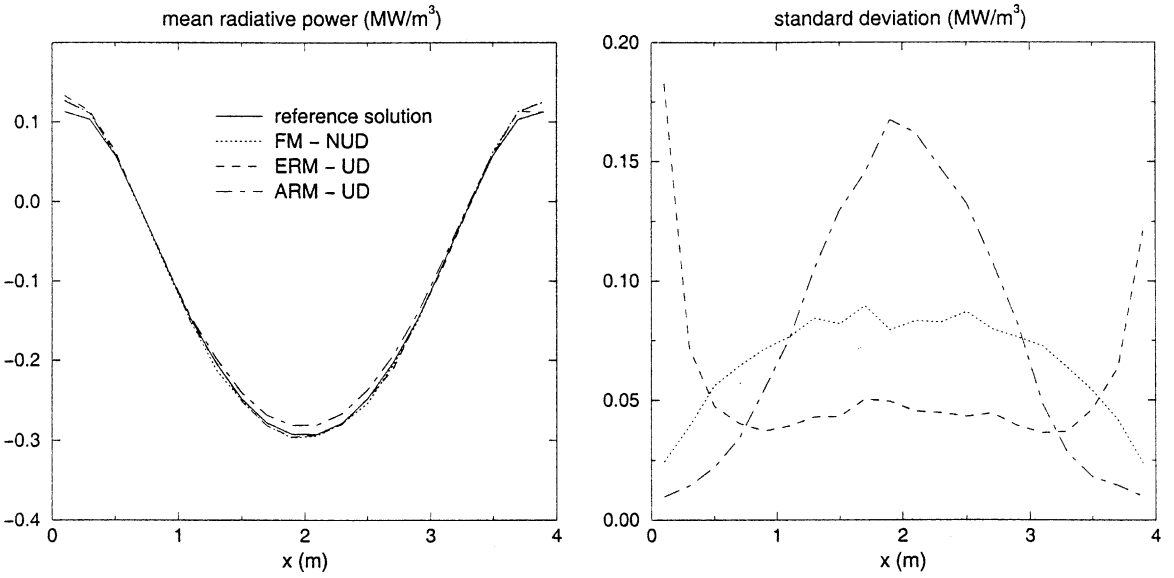

Fig. 13. Mean power value and standard deviation over $N_y N_z$ values of $\widetilde{P}$ (case 7).

proach is a combination of the two reciprocal Monte Carlo formulations. In the central hot zone, the ERM must be used, while in the cold zones close to the walls the ARM approach is more suitable, as illustrated by Fig. 13.

The approaches which give the best results for the radiative powers and the radiative wall fluxes are summarized for all cases in Table 3.

5. Conclusion

Two formulations of the Monte Carlo method based on the reciprocity principle, have been developed and discussed. The reciprocity principle is not only considered from the optical path point of view, as in the reverse Monte Carlo method [30,31], but also from the energy point of view.

One-dimensional benchmark cases involving gray media or actual gas-mixtures and different optical thicknesses and thermal conditions have been defined. In actual gas-mixtures, gas radiative properties are treated in a correlated manner by a CK model. For a given computation time, comparisons have been made between standard deviations on flux and power fields, calculated by the above-mentioned approaches and a conventional forward Monte Carlo method. Although these problems are 1D, the calculations have been carried out with 3D calculation grids in order to check the capacity of the methods for dealing with actual 3D systems.

Advantages and drawbacks of the three approaches have been discussed. In particular, the forward Monte Carlo method appears to be the most suitable for optically thin media, or semi-transparent media characterized by important temperature gradients. On the contrary, the reciprocal formulations are the most suitable for optically thick media or nearly isothermal media. These results have been found for fictitious gray media and actual gas-mixtures. In the general case, the three methods can be used concurrently in order to improve the accuracy by choosing the most suitable method at each point of an actual system.

The results given by the three methods are obtained simultaneously with only one calculation. In terms of computation time, it is not more expensive to obtain the results from the three methods than to obtain the results from only one given method.

Acknowledgements

The authors would like to thank Dr. R. Fournier for helpful discussions.

Appendix A. The CK model

The parameters of the CK model used here have been generated for applications at atmospheric pressure in the temperature range 300–2500 K [46]. The useful wavenumber range (150–9200 cm^{-1}) is divided into 44 spectral bands b for H_2O. However, CO_2 absorbs radiation in only 17 of these bands. Gauss quadratures with 7 points g and g_2 are used for H_2O and CO_2 respectively in their absorption bands, i.e., 49 quadrature points are used in the 17 overlapping bands. Therefore, 1022 pseudo-spectral points have to be considered, which is not a drawback here since a Monte Carlo approach is used.

The expression of the total power emitted by a volume V_i is

$$P_i^{\mathrm{e}} = \sum_{b=1}^{44} \sum_{g=1}^{7} \sum_{g_2=1}^{g_{2max}} \Delta P_i^{\mathrm{e}}(b,g,g_2), \tag{A.1a}$$

$$\Delta P_i^{\mathrm{e}}(b,g,g_2) = 4\pi V_i \left[k_{ibg}^{H_2O} + k_{ibg_2}^{CO_2} \right] I_b^0(T_i)\omega_g \omega_{g_2} \Delta\nu_b, \tag{A.1b}$$

where $k_{ibg}^{H_2O}$ is the pseudo-spectral absorption coefficient of H_2O in V_i and ω_g, ω_{g_2} the weights associated with the quadrature points. For transparency CO_2 bands, $g_{2\max}$ and ω_{g_2} are taken equal to 1. The random generation of a pseudo-spectral point is equivalent to the random generation of the three parameters b, g and g_2. The probability to have these three parameters simultaneously is given by

$$\mathscr{P}(b,g,g_2) = \frac{\Delta P_i^{\mathrm{e}}(b,g,g_2)}{P_i^{\mathrm{e}}}. \tag{A.2}$$

The three parameters b_n, g_n and g_{2_n} are deduced from the generation of only one uniform [0-1] random number R according to the following double inequality

$$\sum_{b=1}^{b_n} \sum_{g=1}^{g_n} \sum_{g_2=1}^{g_{2_n}-1} \mathscr{P}(b,g,g_2) < R \leqslant \sum_{b=1}^{b_n} \sum_{g=1}^{g_n} \sum_{g_2=1}^{g_{2_n}} \mathscr{P}(b,g,g_2). \tag{A.3}$$

References

[1] J.R. Howell, Thermal radiation in participating media: the past the present and some possible futures, J. Heat Transfer 110 (1988) 1220–1229.
[2] R. Viskanta, M.P. Mengüç, Radiation heat transfer in combustion systems, Prog. Energy Combust. Sci. 13 (1987) 97–160.
[3] F.C. Lockwood, N.G. Shah, A new radiation solution method for incorporation in general combustion prediction procedures, in: 18th Symposium (International) on Combustion, The Combustion Institute, Pittsburg, PA, 1981, pp. 1405–1414.
[4] H.C. Hottel, A.F. Sarofim, Radiative Transfer, McGraw-Hill, New York, 1967.
[5] W.A. Fiveland, Discrete ordinates solutions of the radiative transport equation for rectangular enclosures, J. Heat Transfer 106 (1984) 699–706.
[6] W.A. Fiveland, Three-dimensional radiative heat transfer solutions by the discrete ordinates method, J. Thermophys. Heat Transfer 2 (1988) 309–316.
[7] W.A. Fiveland, J.P. Jessee, Comparison of discrete ordinates formulations for radiative heat transfer in multidimensional geometries, J. Thermophys. Heat Transfer 9 (1995) 47–54.
[8] R. Vaillon, M. Lallemand, D. Lemonnier, Radiative heat transfer in orthogonal curvilinear coordinates using the discrete ordinates method, J. Quantitative Spectrosc. Radiative Transfer 55 (1996) 7–17.
[9] M. Sakami, A. Charette, V. Le Dez, Radiative heat transfer in three-dimensional enclosures of complex geom-

etry by using the discrete ordinates method, J. Quantitative Spectrosc. Radiative Transfer 59 (1998) 117–136.
[10] L. Zhang, A. Soufiani, J. Taine, Spectral correlated and non-correlated radiative transfer in a finite axisymmetric system containing an absorbing and emitting real gas–particle mixture, Int. J. Heat Mass Transfer 31 (1988) 2261–2272.
[11] A. Soufiani, J. Taine, Spectrally correlated radiative transfer in real 3D axisymmetrical systems, in: International Symposium on Transport Phenomena, Begell House, 1993, pp. 185–190.
[12] G.D. Raithby, E.H. Chui, A finite volume method for predicting radiant heat transfer in enclosures with participating media, J. Heat Transfer 112 (1990) 415–423.
[13] J.C. Chai, H.S. Lee, S.V. Patankar, Finite volume method for radiation heat transfer, J. Thermophys. Heat Transfer 8 (1994) 419–425.
[14] J.Y. Murthy, S.R. Mathur, Radiative heat transfer in axisymmetric geometries using an unstructured finite volume method, Numer. Heat Transfer, Part B 33 (1998) 397–416.
[15] S.H. Kim, K.Y. Huh, A new angular discretization scheme of the finite volume method for 3-D radiative heat transfer in absorbing emitting and anisotropically scattering media, Int. J. Heat Mass Transfer 43 (2000) 1233–1242.
[16] M.P. Mengüç, R. Viskanta, Radiative transfer in three-dimensional rectangular enclosures containing inhomogeneous anisotropically scattering media, J. Quantitative Spectrosc. Radiative Transfer 33 (1985) 533–549.
[17] A.C. Ratzel, J.R. Howell, Two-dimensional radiation in absorbing–emitting media using the P_N approximation, J. Heat Transfer 105 (1983) 333–340.
[18] J.R. Howell, M. Perlmutter, Monte Carlo solution of thermal transfer through radiant media between gray walls, J. Heat Transfer 86 (1964) 116–122.
[19] J.R. Howell, M. Perlmutter, Monte Carlo solution of radiant heat transfer in a nongrey nonisothermal gas with temperature dependent properties, AIChE J. 10 (1964) 562–567.
[20] A. Haji-Sheikh, E.M. Sparrow, Probability distributions and error estimates for Monte Carlo solutions of radiation problems, Prog. Heat Mass Transfer 2 (1969) 1–12.
[21] J.R. Howell, The Monte Carlo method in radiative heat transfer, J. Heat Transfer 120 (1998) 547–560.
[22] J.T. Farmer, J.R. Howell, Monte Carlo strategies for radiative transfer in participating media, Adv. Heat Transfer 31 (1998) 1–97.
[23] A. Haji-Sheikh, Monte Carlo methods, in: Handbook of Numerical Heat Transfer, Wiley Interscience, New York, 1988, pp. 673–722 (Chapter 16).
[24] L.L. House, L.W. Avery, The Monte Carlo technique applied to radiative transfer, J. Quantitative Spectrosc. Radiative Transfer 9 (1969) 1579–1591.
[25] N. Shamsundar, E.M. Sparrow, R.P. Heinisch, Monte Carlo radiation solutions – effect of energy partitioning and number of rays, Int. J. Heat Mass Transfer 16 (1973) 690–694.
[26] M. Kobiyama, Reduction of computing time and improvement of convergence stability of the Monte Carlo method applied to radiative heat transfer with variable properties, J. Heat Transfer 111 (1989) 135–140.
[27] W.R. Martin, G.C. Pomraning, Monte Carlo analysis of the backscattering of radiation from a sphere to a plane, J. Quantitative Spectrosc. Radiative Transfer 43 (1990) 115–126.
[28] K. Kudo, H. Taniguchi, A. Kuroda, M. Ohtaka, H. Kakota, Improvement of analytical method on radiative heat transfer in nongrey media by Monte Carlo method, Heat Transfer – Jpn. Res. 22 (1993) 559–572.
[29] S.T. Surzhikov, J.R. Howell, Monte Carlo simulation of radiation in scattering volumes with line structure, J. Thermophys. Heat Transfer 12 (1998) 278–281.
[30] D.V. Walters, R.O. Buckius, Rigorous development for radiation heat transfer in nonhomogeneous absorbing emitting and scattering media, Int. J. Heat Mass Transfer 35 (1992) 3323–3333.
[31] D.V. Walters, R.O. Buckius, Monte Carlo methods for radiative heat transfer in scattering media, in: C.-L. Tien (Ed.), Annual Review of Heat Transfer, vol. 5, CRC Press, Boca Raton, 1994, pp. 131–176 (Chapter 3).
[32] R. Fournier, Rayonnement thermique dans les gaz: Analyse du couplage avec la convection naturelle, Thèse de doctorat, Université Paul Sabatier, Toulouse, France 1994.
[33] M. Cherkaoui, J.-L. Dufresne, R. Fournier, J.-Y. Grandpeix, A. Lahellec, Monte Carlo simulation of radiation in gases with a narrow-band model and a net-exchange formulation, J. Heat Transfer 118 (1996) 401–407.
[34] M. Cherkaoui, J.-L. Dufresne, R. Fournier, J.-Y. Grandpeix, A. Lahellec, Radiative net-exchange formulation within one-dimensional gas enclosures with reflective surfaces, J. Heat Transfer 120 (1998) 275–278.
[35] A. de Lataillade, J.-L. Dufresne, M. El Hafi, V. Eymet, R. Foumier, A net exchange Monte Carlo approach to radiation in optically thick systems. J. Quantitative Spectrosc. Radiative Transfer, accepted 2002.
[36] H.A.J. Vercammen, G.F. Froment, An improved zone method using Monte Carlo techniques for the simulation of radiation in industrial furnaces, Int. J. Heat Mass Transfer 23 (1980) 329–337.
[37] J.T. Farmer, J.R. Howell, Hybrid Monte Carlo/diffusion methods for enhanced solution of radiative transfer in optically thick nongrey media, Radiative Heat Transfer: Curr. Res., ASME HTD 276 (1994) 203–212.
[38] J.T. Farmer, J.R. Howell, Monte Carlo algorithms for predicting radiative transfer in optically thick participating media, in: Tenth International Heat Transfer Conference, vol. 2, Taylor & Francis, Brighton, UK, 1994, pp. 37–42.
[39] S.W. Baek, D.Y. Byun, S.J. Kang, The combined Monte Carlo and finite volume method for radiation in a two-dimensional irregular geometry, Int. J. Heat Mass Transfer 43 (2000) 2337–2344.
[40] J. Taine, A. Soufiani, Gas IR radiative properties: from spectroscopic data to approximate models, Adv. Heat Transfer 33 (1999) 295–414.
[41] J. Liu, S.N. Tiwari, Investigation of radiative transfer in nongrey gases using a narrow band model and Monte Carlo simulation, J. Heat Transfer 116 (1994) 160–166.
[42] R. Goody, R. West, L. Chen, D. Crisp, The correlated-k method for radiation calculations in nonhomogeneous atmospheres, J. Quantitative Spectrosc. Radiative Transfer 42 (1989) 539–550.

[43] A.A. Lacis, V. Oinas, A description of the correlated-k distribution method for modeling nongrey gaseous absorption thermal emission and multiple scattering in vertically inhomogeneous atmospheres, J. Geophys. Res. 96 (1991) 9027–9063.

[44] P. Rivière, A. Soufiani, J. Taine, Correlated-k and fictitious gas methods for H_2O near 2.7 μm, J. Quantitative Spectrosc. Radiative Transfer 48 (1992) 187–203.

[45] P. Rivière, A. Soufiani, J. Taine, Correlated-k fictitious gas model for H_2O infrared radiation in the Voigt regime, J. Quantitative Spectrosc. Radiative Transfer 53 (1995) 335–346.

[46] A. Soufiani, J. Taine, High temperature gas radiative property parameters of statistical narrow-band model for H_2O, CO_2 and CO and correlated-k model for H_2O and CO_2, Int. J. Heat Mass Transfer 40 (1997) 987–991.

[47] J. Taine, J.-P. Petit, Transferts Thermiques, Dunod, third ed., to be published.

[48] R. Siegel, J.R. Howell, Thermal Radiation Heat Transfer, third ed., Taylor & Francis, Washington, DC, 1992.

[49] P. L'Ecuyer, Good parameter sets for combined multiple recursive random number generators, Oper. Res. 47 (1999) 159–164. Available from <http://www.iro.umontreal.ca/~lecuyer/papers.html> (files combmrg2.ps and combmrg2.c).

[50] L. Pierrot, P. Rivière, A. Soufiani, J. Taine, A fictitious-gas-based absorption distribution function global model for radiative transfer in hot gases, J. Quantitative Spectrosc. Radiative Transfer 62 (1999) 609–624.